Semiconducting ZnSnN2 thin films for Si/ZnSnN2 p-n junctions

Ruifeng Qin, Hongtao Cao, Lingyan Liang, Yufang Xie, Fei Zhuge, Hongliang Zhang, Junhua Gao, Kashif Javaid , Caichi Liu, and Weizhong Sun

Citation: Applied Physics Letters **108**, 142104 (2016); doi: 10.1063/1.4945728
View online: http://dx.doi.org/10.1063/1.4945728
View Table of Contents: http://scitation.aip.org/content/aip/journal/apl/108/14?ver=pdfcov
Published by the AIP Publishing

Semiconducting $ZnSnN_2$ thin films for Si/$ZnSnN_2$ p-n junctions

Ruifeng Qin,[1,2] Hongtao Cao,[2] Lingyan Liang,[2,a)] Yufang Xie,[2] Fei Zhuge,[2] Hongliang Zhang,[2] Junhua Gao,[2] Kashif Javaid,[2] Caichi Liu,[1] and Weizhong Sun[1,a)]
[1]*Hebei Engineering Laboratory of Photoelectronic Functional Crystals, Hebei University of Technology (HEBUT), Tianjin 300401, People's Republic of China*
[2]*Ningbo Institute of Material Technology and Engineering, Chinese Academy of Sciences, and Key Laboratory of Additive Manufacturing Materials of Zhejiang Province, Ningbo 315201, People's Republic of China*

(Received 27 October 2015; accepted 25 March 2016; published online 6 April 2016)

$ZnSnN_2$ is regarded as a promising photovoltaic absorber candidate due to earth-abundance, non-toxicity, and high absorption coefficient. However, it is still a great challenge to synthesize $ZnSnN_2$ films with a low electron concentration, in order to promote the applications of $ZnSnN_2$ as the core active layer in optoelectronic devices. In this work, polycrystalline and high resistance $ZnSnN_2$ films were fabricated by magnetron sputtering technique, then semiconducting films were achieved after post-annealing, and finally Si/$ZnSnN_2$ p-n junctions were constructed. The electron concentration and Hall mobility were enhanced from 2.77×10^{17} to $6.78 \times 10^{17}\,cm^{-3}$ and from 0.37 to $2.07\,cm^2\,V^{-1}\,s^{-1}$, corresponding to the annealing temperature from 200 to 350 °C. After annealing at 300 °C, the p-n junction exhibited the optimum rectifying characteristics, with a forward-to-reverse ratio over 10^3. The achievement of this $ZnSnN_2$-based p-n junction makes an opening step forward to realize the practical application of the $ZnSnN_2$ material. In addition, the nonideal behaviors of the p-n junctions under both positive and negative voltages are discussed, in hope of suggesting some ideas to further improve the rectifying characteristics. © *2016 AIP Publishing LLC*. [http://dx.doi.org/10.1063/1.4945728]

To meet the world economic growth demand by 2050, it requires over 20 TW (10^{12} W) new power instead of fossil fuel to maintain the atmospheric CO_2 concentrations at their current level.[1] Solar photovoltaics (PV) are considered as one of the most promising options for a low-carbon future.[1–3] In addition to silicon-based PV, aggressive development of non-silicon based PV materials (such as CdTe and $CuInGaSe_2$) has greatly inspired confidence in reducing PV module price per watt by increasing the photoelectric conversion efficiency or/and using inexpensive materials.[4] For example, the CdTe and $CuInGaSe_2$ technologies are still suffering serious problems of toxicity (Cd) or rarity (Te ~ 0.005 ppm, In ~ 0.048 ppm, and Se ~ 0.05 ppm) for TW-scale deployment.[5,6] Thus, it becomes more and more imperative to develop new PV technology based on environmentally friendly materials which are earth-abundant (i.e., new-generation earth-abundant solar PV[7]).

$ZnSnN_2$, a member of ternary Zn-IV(Si, Ge, Sn)-N_2 semiconductors,[8–11] has attracted much attention because of its potential application in new-generation earth-abundant solar PV. This material has many favorable characteristics. (I) Zn, Sn, and N elements are non-toxic, earth–abundant (Zn ~ 75 ppm, Sn ~ 2.2 ppm), and recyclable.[12] (II) $ZnSnN_2$ possesses a sound absorption coefficient ranging from ultraviolet to near infrared region of electromagnetic spectrum, comparable to some typical photovoltaic materials such as GaAs, CdTe, and InP.[13] (III) $ZnSnN_2$ has a tunable direct band gap (1.0–2.0 eV) due to cation disorder,[4,12,14] especially showing a reasonably predictive value of 1.4 eV and an experimental value of 1.6–1.7 eV which, respectively, meets the requirement for a single junction cell and the top cell in a two-junction device.[4] However, the previous investigations demonstrated that $ZnSnN_2$ is a n-type degenerated semiconductor, in which the carrier concentration is up to $10^{20}\,cm^{-3}$ so as to limit its application as an active semiconductor layer.[12,15] Thus far, there are no reports on $ZnSnN_2$-based device applications such as p-n junctions and Schottky diodes. In this work, we investigated the influence of post-annealing temperature on the structural, morphological, electrical, and optical properties of DC-magnetron-sputtered $ZnSnN_2$ films. The annealed films exhibited n-type semiconductor characteristics, with an electron concentration in the magnitude of $10^{17}\,cm^{-3}$, which facilitates the construction of Si/$ZnSnN_2$ p-n junctions with a significant rectifying effect.

$ZnSnN_2$ films were prepared on quartz glasses and p-type Si wafers (with a resistivity of $1.4 \times 10^{-3}\ \Omega$ cm and a hole concentration of $5.4 \times 10^{19}\,cm^{-3}$) by DC-magnetron sputtering at room temperature. Before being loaded into the vacuum chamber, the substrates were ultrasonically cleaned successively in acetone, ethanol, and deionized water, and then dried in pure N_2 flow. Later on, 5% HF solution was employed to remove the surface oxide layer on the Si wafer. The distance from the target to the substrate was ~8 cm and the sputtering gun was inclined at ~20° to the substrate normal. The base pressure was $\sim 6 \times 10^{-4}$ Pa. The alloy target with weight ratio of Zn:Sn = 3:2 was used as the source material. (The purity of both Zn and Sn are 99.99%.) The sputtering gas N_2 (5 N in purity) fixed at 10 sccm was controlled by a mass flow controller to maintain the working pressure at 2.0 Pa. $ZnSnN_2$ films with a thickness about 130 nm were fabricated by using a sputtering power of 120 W. For the fabrication of p-Si/n-$ZnSnN_2$ heterojunctions, the patterning was achieved with the help of standard photolithography process using AR-P 5350 as photoresist and AR 300–26 as developer. Afterwards, the

a)Authors to whom correspondence should be addressed. Electronic addresses: lly@nimte.ac.cn and swz@hebut.edu.cn

$ZnSnN_2$ films were wet-etched using HF and $NH_3 \cdot H_2O$ mixed solution. Then, Ni (50 nm)/Au(20 nm) electrodes were deposited on both $ZnSnN_2$ and Si using an electron beam evaporation system. Finally, the films and the p-n junctions were subjected to a thermal annealing in N_2 atmosphere for 3 h at 200 °C, 300 °C, and 350 °C. Additionally, two strip-shaped Ni/Au electrodes were also deposited on Si and some $ZnSnN_2$/quartz films followed by the same annealing treatment, in order to check the electrode/semiconductor contact. (The schematic structure and measured results are depicted in Fig. S1 in the supplementary material.[16]) The measured linear I-V curves confirm that the Ni/Au electrode is in ohmic contact with both p-Si and $ZnSnN_2$, which ensures that the rectifying characteristics discussed in the following text are attributed to the Si/$ZnSnN_2$ p-n junction rather than the metal/semiconductor Schottky contact.

The phase composition of the films was characterized by X-ray diffraction (XRD, Bruker D8 advance X-ray diffractometer). The surface morphologies of the films were investigated by scanning electron microscope (SEM, Hitachi S4800). Energy dispersive X-ray facility (EDX, Oxford X-max) attached to the SEM setup was used for oxygen content analysis. The absorption properties and film thickness were analyzed by a variable angle spectroscopic ellipsometry (M-2000DI, J. A. Woollam Inc.) in the photon energy ($h\nu$) ranging from 0.73 to 6.20 eV. The film electrical properties were examined by Hall-effect measurement system (HP-5500 C, American Nanometrics). The current-voltage (I-V) properties of the p-n junctions were performed at room temperature in the dark via a semiconductor characterization system (Keithley 4200).

Figure 1 shows the θ–2θ XRD patterns in the 2θ region of 25°–75°. Seven discernible peaks located at 30.6°, 32.7°, 34.9°, 45.8°, 54.7°, 60.0°, and 65.0° are observed for the as-deposited and annealed films, consistent with the wurtzite-like $ZnSnN_2$.[4,15] By increasing the annealing temperature, the intensity of the 32.7° peak corresponding to the (0001) crystal direction is increased slightly, as confirmed by the fact that the average grain size estimated by the Scherrer formula is changed from 13.1 to 14.7 nm. It is also reported by Fioretti *et al.*[4] that post-annealing treatment on $ZnSnN_2$ thin films could promote the (0001) preferential growth. In other words, it is suggested that polycrystalline $ZnSnN_2$ thin films can be synthesized even at room temperature, but further grain growth requires a post-annealing temperature higher than 350 °C or a longer annealing duration. Further efforts to improve the crystal quality are still in progress in our group. Figure 2 displays the SEM images of the $ZnSnN_2$ films on Si wafer with different annealing temperatures. All these films illustrate smooth and homogeneous surface morphology. No distinct grain growth is observed at different annealing temperatures, in a good agreement with the XRD observations.

Generally, metal nitrides films would contain oxygen. The oxygen content in $ZnSnN_2$ films on Si wafer is determined to be 7.69%, 9.13%, 9.99%, 10.86% for the as-deposited and the 200 °C, 300 °C, 350 °C-annealed $ZnSnN_2$ films by EDX, respectively. The relatively high oxygen content could originate from residual oxygen in the growth process and adsorbed H_2O and O_2 on the film surface after exposure to the ambient air. No peaks assigned to oxygen-related phases are observed in XRD patterns probably due to their amorphous states, since the foreign element (O) usually boosts the microstructural disorder in $ZnSnN_2$. Post-annealing in N_2 may also induce further oxidation because of our not-well-sealed furnace, so the oxygen content shows an increasing trend with the temperature.

The absorption coefficient (α) can be obtained by spectroscopic ellipsometry modeling (the details have been reported elsewhere[13]), as shown in the inset of Fig. 3. All α spectra have a relatively steep absorption edge, and the absorption edge exhibits a small blue-shift with the increasing annealing temperature. The $(\alpha h\nu)^2$ *vs.* $h\nu$ plot (Fig. 3) is generally adopted to extract the direct optical band gap. It is revealed that the as-deposited and annealed films have the band gap of ~1.64 eV and ~1.70 eV, respectively, in line with the blue-shift of absorption edge after annealing. This factor has approached the ideal band gap for solar energy harvesting.

The electrical properties of the films were repetitively tested by the Hall-effect measurement (the testing details are given in Fig. S2[16]), and the statistical results are listed in Table I. In contrast to high conductivity character reported in other literatures, the as-deposited film exhibited a high resistivity beyond the measurement limit. The resistivity is

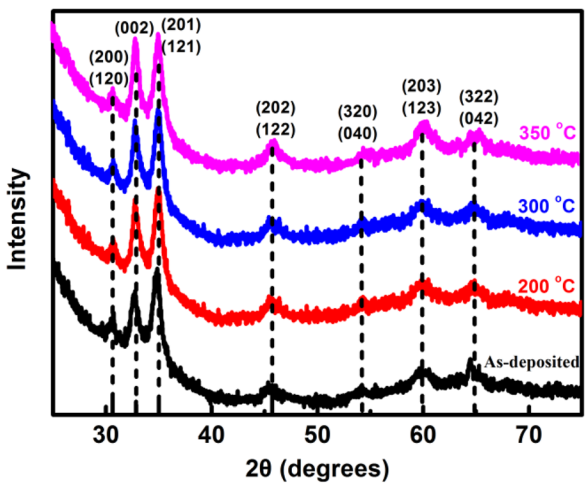

FIG. 1. XRD patterns with Miller indices of the as-deposited and annealed $ZnSnN_2$ films.

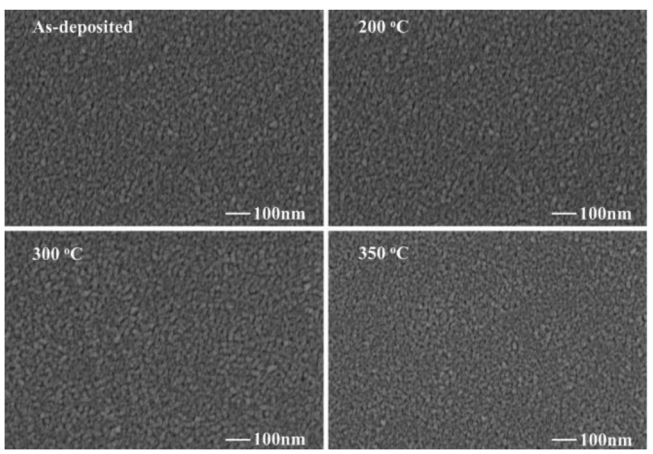

FIG. 2. SEM images of $ZnSnN_2$ films on Si with different annealing temperatures.

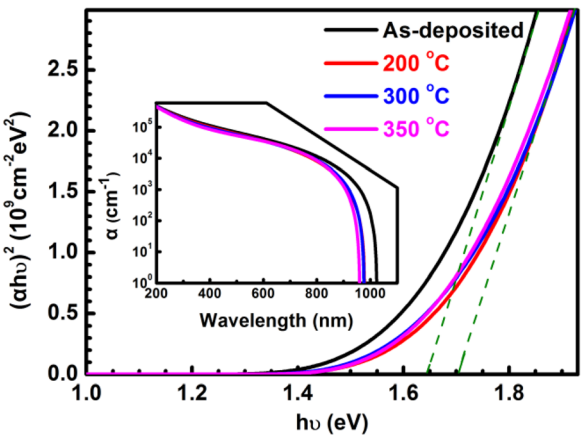

FIG. 3. Plots of $(\alpha h\nu)^2$ *vs.* $h\nu$ of the $ZnSnN_2$ films. The inset shows absorption coefficient spectra.

TABLE I. Hall-effect measurement results of the fabricated $ZnSnN_2$ films.

Annealing temperature (°C)	Resistivity (Ω cm)	Mobility ($cm^2\ V^{-1}\ s^{-1}$)	Electron concentration (cm^{-3})
0	$>10^2$	…	…
200	61.26	0.37	2.77×10^{17}
300	17.03	1.29	2.85×10^{17}
350	4.61	2.07	6.78×10^{17}

decreased after annealing (down to 4.61 Ω cm at 350 °C), due to an increase in both mobility (0.37–2.07 $cm^2\ V^{-1}\ s^{-1}$) and electron concentration (2.77–6.78 × 10^{17} cm^{-3}). The increase of the electron concentration with annealing temperatures is probably related to the increasing oxygen content, as supported by the first-principles calculations that oxygen can substitute nitrogen to form O_N antisites acting as donors in $ZnSnN_2$.[11] Anyway our annealed samples obviously demonstrate semiconductor characteristics. The tunable electrical properties, in particular, the carrier concentration, would pave a way to construct electronic or optoelectronic devices.

Si/$ZnSnN_2$ p-n junctions (as schematically shown in the inset of Fig. 4(a)) were fabricated at room temperature, and then the as-deposited devices were treated with the same annealing conditions as those of the films. The as-deposited p-n junctions do not show any rectifying effect (as shown in Fig. S3[16]), probably due to the high resistivity of the unannealed $ZnSnN_2$ films. After annealing, however, the p-n junctions demonstrate clear rectifying effect, as illustrated that the reverse currents are small while the forward currents increase exponentially after tuning-on (Fig. 4(a)). As the annealing temperature increases from 200 to 350 °C, the turn-on voltage decreases from 1.53 to 1.39 V. The forward-to-reverse current ratio is up to 1066 at ±1.5 V for the device annealed at 300 °C, while those of the 200 °C- and 350 °C-annealed p-n junctions are 123 and 81, respectively. Next, the reasons for this variation will be further discussed.

The reverse *I-V* curves in double-logarithmic scale are shown in Fig. 4(b). According to the fitting results, the charge transport behaviors of the three p-n junctions mainly follow the trap-controlled space charge limited conduction (SCLC) mechanism (i.e., $I \propto V^m$), which can be divided into three portions: (i) $m \approx 1$ under low voltage; (ii) $m \approx 2$, moderate voltage; and (iii) $m \gg 2$, high voltage. The SCLC is governed by single-level shallow traps when $m = 2$, and by exponentially distributed traps when $m > 2$. For the latter case, the functional form of SCLC current can be given by $I = (sq^{1-l}\mu_n N_c / d^{2l+1})((2l+1)/(l+1))^{l+1}(\varepsilon_0\varepsilon_r l/N_t(l+1))^l V^{l+1}$,[17] where s is the device area, μ_n the electron mobility, ε_0 the permittivity of free space, ε_r the static dielectric constant, q the electronic charge, N_c the density of the states in the conduction band, N_t the total density of traps, and $l = T_c/T$ (T_c is a characteristic

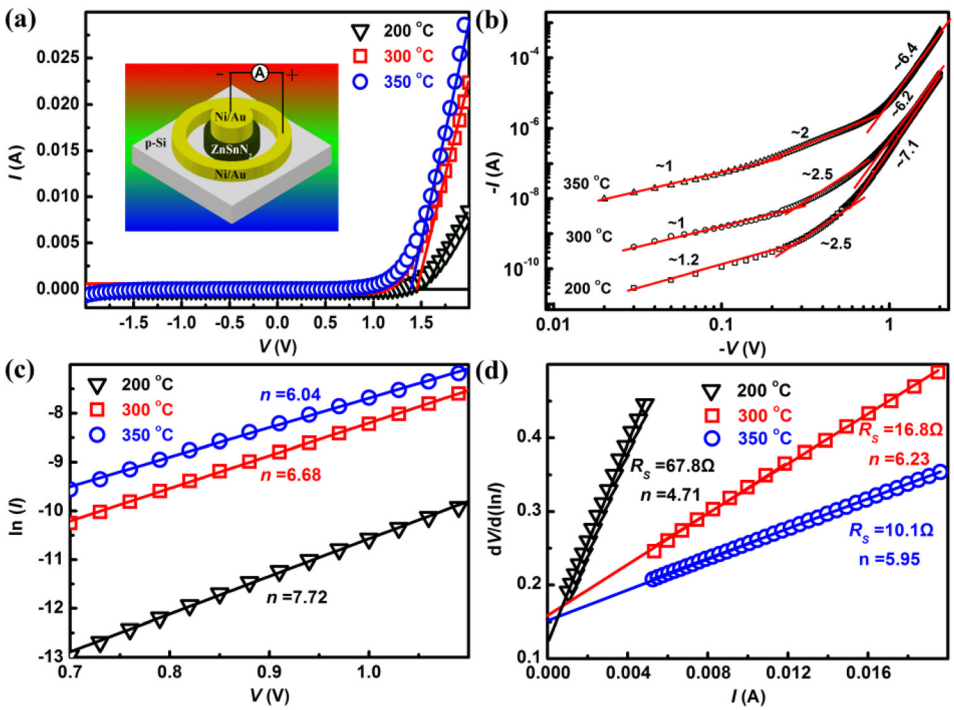

FIG. 4. (a) *I-V* curves of the Si/$ZnSnN_2$ p-n junctions annealed at different temperatures. The inset is schematic diagram of the Si/$ZnSnN_2$ p-n junctions. (b) The experimental and fitting reverse *I-V* curves in double-logarithmic scale. (c) The experimental and fitting ln(*I*)-*V* curves. (d)The experimental and fitting $\frac{\partial V}{\partial \ln(I)}$ *vs.* *I* curves.

temperature related to the trap distribution). It is noted that, here, d is the width of the depletion region in the p-n junction and is roughly proportional to $N_n^{-1/2}$ when $N_n \ll N_p$ (N_n and N_p are the carrier concentration in the $ZnSnN_2$ film and Si wafer, respectively). Thus, the SCLC current $I \propto N_n^{(2l+1)/2}$, which means that the current would be highly sensitive to the carrier concentration of the $ZnSnN_2$ films (here $l \sim 5$–6 based on the fitting results). According to our Hall measurement results, the electron concentrations of the 200 and 300 °C films are very similar while less than a half of that of the 350 °C films. Hence, the reverse current of the 350 °C annealed devices is dozens of times higher than that of the other two counterparts, resulting in a small forward-to-reverse current ratio.

Conventional thermionic emission model is used to extract the diode parameters of p-n junctions, as expressed by[18]

$$I = I_0\left[\exp\left(\frac{qV}{nkT}\right) - 1\right], \tag{1}$$

where q, n, T, V, k, and I_0 represents the charge of electron, ideality factor, absolute temperature, biasing voltage, Boltzmann constant, and the reverse saturation current, respectively. The ideality factor n can be obtained from the linear region slope of ln(I)–V plot, as shown in Fig. 4(c). The ideality factor is calculated to be 7.72, 6.68, and 6.04 for the 200 °C, 300 °C, and 350 °C-annealed devices, respectively. High ideality factor (1.0 for an ideal p-n junction) generally originates from the presence of inter diffusion, highly strained interface, structural imperfections (such as grain boundaries), or high series resistance (R_s),[19–22] etc. The ideality factor can also be derived according to the following relationship,[22]

$$I = I_0 \exp\left[\frac{q(V - IR_S)}{nkT}\right]. \tag{2}$$

The above equation can be further developed as follow:[21]

$$\frac{\partial V}{\partial \ln(I)} = \frac{nkT}{q} + IR_S. \tag{3}$$

The plot of $\frac{\partial V}{\partial \ln(I)}$ *vs.* I should be linear, in which the slope and intercept represent R_s and n, respectively. In this model, the effect of series resistance was considered. Hence, one can determine the influence of series resistance on the rectifying characteristics through comparing the ideality factors derived by this model and the ideal thermionic emission model. The $\frac{\partial V}{\partial \ln(I)}$ *vs.* I plots are illustrated in Fig. 4(d), showing excellent linearity. With increasing the annealing temperature, the series resistance is decreased from 67.8 to 10.2 Ω, which is in a good agreement with the decreasing resistivity of the $ZnSnN_2$ films (as illustrated in Table I). The ideality factor is extracted to be 4.71, 6.23, and 5.95 for the 200 °C, 300 °C, and 350 °C-annealed junctions, respectively, smaller than those corresponding values extracted by the ideal thermionic emission model. Interestingly, the ideality factor of the 200 °C-annealed device drops a lot (from 7.72 to 4.71), while those of the devices with higher annealing temperatures decrease a little. It implies that high series resistance is one of important reasons for the moderate performance of the 200 °C-annealed junction, while some other factors such as element inter-diffusion at $ZnSnN_2$/Si interface should be dominant for the 300 °C and 350 °C-annealed devices. Annealing treatment at high temperatures brings about a tradeoff between series resistance and interface quality. Further efforts are still ongoing to decrease the series resistance and improve the interface quality.

In summary, polycrystalline $ZnSnN_2$ films and the heterostructure p-n junctions were fabricated by DC-magnetron sputtering. The structural, morphological, optical, and electrical properties of the $ZnSnN_2$ films were investigated as a function of the post-annealing temperature. By increasing annealing temperature from 0 to 350 °C, the optical bandgap was adjusted from 1.64 to 1.70 eV and the resistivity was regulated from high resistivity to 4.61 Ω cm. The semiconductor characteristics of the annealed films were obtained, as seen that the electron concentration and the electron mobility were in the range of 2.77–6.78 × 10^{17} cm^{-3} and 0.37–2.07 cm^2 V^{-1} s^{-1}, respectively. Finally, p-n junctions with sound rectifying effect have been achieved by applying these semiconducting films. These results reveal that semiconducting films can be synthesized experimentally, which has broken the theoretical prediction that the $ZnSnN_2$ material always displays a metallic conductivity.[11] Furthermore, the achievement of the p-n junctions demonstrates that the $ZnSnN_2$ material has an excellent potential utilized as the core active layer in electronic and optoelectronic devices.

This work is supported by the Natural Science Foundation of Zhejiang Province (LY16F040002), National Basic Research Program of China (2012CB933003), and the Natural Science Foundation of Ningbo (2015A610043).

[1]T. M. Razykov, C. S. Ferekides, D. Morel, E. Stefanakos, H. S. Ullal, and H. M. Upadhyaya, Sol. Energy **85**(8), 1580–1608 (2011).
[2]A. Goetzberger, C. Hebling, and H.-W. Schock, Mater. Sci. Eng. R **40**, 1–46 (2003).
[3]B. Parida, S. Iniyan, and R. Goic, Renewable Sustainable Energy Rev. **15**(3), 1625–1636 (2011).
[4]A. N. Fioretti, A. Zakutayev, H. Moutinho, C. Melamed, J. D. Perkins, A. G. Norman, M. Al-Jassim, E. S. Toberer, and A. C. Tamboli, J. Mater. Chem. C **3**, 11017 (2015).
[5]N. Asim, K. Sopian, S. Ahmadi, K. Saeedfar, M. A. Alghoul, O. Saadatian, and S. H. Zaidi, Renewable Sustainable Energy Rev. **16**(8), 5834–5847 (2012).
[6]M. Edoff, Ambio **41**, 112–118 (2012).
[7]C. Wadia, A. P. Alivisatos, and D. M. Kammen, Environ. Sci. Technol. **43**(6), 2072–2077 (2009).
[8]T. R. Paudel and W. R. L. Lambrecht, Phys. Rev. B **78**(11), 115204 (2008).
[9]T. R. Paudel and W. R. L. Lambrecht, Phys. Rev. B **79**(24), 245205 (2009).
[10]A. Punya, W. R. L. Lambrecht, and M. V. Schilfgaarde, Phys. Rev. B **84**(16), 165204 (2011).
[11]S. Y. Chen, P. Narang, H. A. Atwater, and W. W. Lin, Adv. Mater. **26**(2), 311–315 (2014).
[12]N. Feldberg, J. D. Aldous, W. M. Linhart, L. J. Phillips, K. Durose, P. A. Stampe, R. J. Kennedy, D. O. Scanlon, G. Vardar, R. L. Field III, T. Y. Jen, R. S. Goldman, T. D. Veal, and S. M. Durbin, Appl. Phys. Lett. **103**(4), 042109 (2013).
[13]F. L. Deng, H. T. Cao, L. Y. Liang, J. Li, J. H. Gao, H. L. Zhang, R. F. Qin, and C. C. Liu, Opt. Lett. **40**(7), 1282–1285 (2015).
[14]P. C. Quayle, K. L. He, J. Shan, and K. Kash, MRS Commun. **3**(3), 135–138 (2013).
[15]L. Lahourcade, N. C. Coronel, K. T. Delaney, S. K. Shukla, N. A. Spaldin, and H. A. Atwater, Adv. Mater. **25**(18), 2562–2566 (2013).
[16]See supplementary material at http://dx.doi.org/10.1063/1.4945728 for schematic diagram and I-V curves of electrode/$ZnSnN_2$/electrode and

electrode/Si/electrode structures, testing details of Hall measurement, I-V curves of as-deposited p-n junctions.
[17]R. B. Pan, J. Li, F. Zhuge, L. Q. Zhu, L. Y. Liang, H. L. Zhang, J. H. Gao, H. T. Cao, B. Fu, and K. Li, Appl. Phys. Lett. **108**, 013504 (2016).
[18]S. K. Cheung and N. W. Cheung, Appl. Phys. Lett. **49**(2), 85 (1986).
[19]S. Sharma and C. Periasamy, Superlattice Microstruct. **73**, 12–21 (2014).
[20]S. Hussain, C. B. Cao, W. S. Khan, G. Nabi, Z. Usman, A. Majid, T. Alharbi, Z. Ali, F. K. Butt, M. Tahir, M. Tanveer, and F. Idress, Mater. Sci. Semicond. Process **25**, 181–185 (2014).
[21]X. X. Li, L. Y. Liang, H. T. Cao, R. F. Qin, H. L. Zhang, J. H. Gao, and F. Zhuge, Appl. Phys. Lett. **106**(13), 132102 (2015).
[22]R. K. Gupta, K. Ghosh, and P. K. Kahol, Physica E **41**(4), 617–620 (2009).